Low Elevation Transmission Measurements at EOPACE
Part I: Molecular and Aerosol Effects

Carl Zeisse[a], Stuart Gathman[a], Douglas Jensen[a], Kathleen Littfin[a], Bill Moision[a], Ken Davidson[b], Paul Frederickson[b], Arie de Jong[c], Peter Fritz[c], Gerritt de Leeuw[c], J. Luc Forand[d], and Denis Dion[d]

[a]NCCOSC RDTE DIV D883 (NRaD), 49170 Propagation Path, San Diego, CA 92152-7385
[b]Naval Postgraduate School, Code 63 DS, 589 Dyer Road Room 252, Monterey, CA 93493-5000
[c]Physics and Electronics Laboratory TNO, PO Box 96864, 2509 JG The Hague, The Netherlands
[d]Defence Research Establishment Valcartier (DREV), 2459 Pie XI Blvd., North, Val-Bélair, Québec, Canada G3J 1X5

ABSTRACT

An analysis is presented showing the effects of molecules and aerosols on atmospheric transmission data obtained during the Electro-Optical Propagation Assessment in Coastal Environments (EOPACE) campaign carried out in San Diego during March and April, 1996. Mid wave infrared transmission was measured over San Diego Bay along a 14.9 km path and a 7.0 km path at heights less than 4 meters above the water. Simultaneous meteorological measurements were obtained from two buoys placed at the mid-points of each path. An aerosol spectrometer was used to measure the aerosol size distribution over each transmission path. Data were analyzed with MODTRAN and Mie theory. The conclusion of this and the next two papers is that low altitude infrared transmission is a complex phenomenon whose mean value may be controlled either by molecular absorption, aerosol scattering, or refractive focusing, and whose fluctuating value is controlled by scintillation.

Keywords: infrared, transmission, extinction, molecule, aerosol, refraction, scintillation, EOPACE

1. INTRODUCTION

We are interested in atmospheric transmission in the infrared very close to the surface of the ocean in coastal regions where aerosols and refraction play more important roles than molecules. It will become evident after this series of papers[1,2] that infrared transmission under these conditions is a much more complex phenomenon than it is at higher altitudes in the troposphere and stratosphere.

1.1 Molecules

A striking feature of molecular absorption is the large, rapid variation of absorption cross-section with spectral wave number. The rather weak absorption in certain spectral bands causes the well known near, mid, and long wave infrared window regions. The extremely strong absorption in other spectral bands must be taken into account in the design of infrared instruments and may be revealed, for example, in dips in the relative spectral responsivity of an infrared instrument[3] due to short (tens of cm) optical paths through air within the instrument body. A mere 1 m of clear air is enough to reduce the transmission to 50% at 2400 cm^{-1} where carbon dioxide absorbs and at 1500 and 3700 cm^{-1} where water vapor absorbs. Yet even 20 km of clear air is not enough to reduce the transmission very much below 30% inside the mid wave window between 2500 and 3300 cm^{-1}.

These transmission examples were taken from MODTRAN, a computer program[4] developed by the Air Force to predict the transmission and radiance of the atmosphere. The predictions of MODTRAN are widely used and particularly convenient for spectral conditions broader than a natural molecular line width (0.01 to 0.1 cm^{-1}), which means almost all conditions except those which involve lasers. The reason is that there is no simple law which relates *broad band* transmission to range. At a single wave number v, there is a simple law, Beer's Law, according to which molecular transmission τ_m decays exponentially with path length L (km):

$$\tau_m(v, L) = \exp\left\{-\beta_m(v)L\right\} \tag{1}$$

Here $\beta_m(v)$ is the molecular extinction coefficient (km^{-1}) at wave number v (cm^{-1}). It is practically impossible to measure radiation transmitted at a single wave number. For a narrow spectral band Δv, the monochromatic result given above must be averaged over the band:

$$\bar{\tau}_m(\Delta v, L) = \frac{1}{\Delta v}\int \tau_m(v)\,dv = \frac{1}{\Delta v}\int \exp\left\{-\beta_m(v)L\right\}\,dv \tag{2}$$

More generally, when a broad band instrument with spectral responsivity $f(v)$ is used to measure transmittance, equation (2) is generalized to

$$\bar{\tau}_m(f, L) = \frac{\int \exp\left\{-\beta_m(v)L\right\} f(v)\,dv}{\int f(v)\,dv} \tag{3}$$

If the extinction coefficient were constant or slowly varying over the band, it could be removed from the integrals in (2) and (3) and Beer's Law would continue to hold approximately for the band as well as exactly for the single wave number. That is generally the case for aerosol extinction but, unfortunately, not the case for molecular extinction. Molecular extinction varies greatly when the wave number is changed slightly. Since an integral is a sum, and since the sum of two exponentials is not an exponential, the molecular transmittance observed with a broad band instrument does not obey Beer's Law[5]. In equation form,

$$\bar{\tau}_m(f, L) = \frac{\int \exp\left\{-\beta_m(v)L\right\} f(v)\,dv}{\int f(v)\,dv} \neq \exp\left\{-\bar{\beta}_m L\right\} \tag{4}$$

where the bar over the extinction coefficient symbolizes its average value over the band. Hence a numerical calculation of broad band transmission is convenient.

1.2 Aerosols

Aerosols, for example volcanic ash, play a major role throughout the stratosphere and troposphere, but very little is known about the composition of aerosols at very low elevations within meters of the ocean surface or above breaking surf. In coastal regions, further complications arise because man made pollutants may be present depending on their generation rate and the wind direction. If man made pollutants, dense coastal fog, or heavy surf is present along only part of a transmission path, it will seriously invalidate the common assumption (which we will also make) that conditions are homogeneous along the entire path. However, we *are* fortunate with respect to aerosols in that, for the broad bands we encounter, Beer's Law remains a good approximation due to the smooth variation of aerosol extinction with wave number. We may assume that aerosol transmission τ_a is given by

$$\bar{\tau}_a(f, L) \approx \exp\left\{-\bar{\beta}_a L\right\} \tag{5}$$

where $\bar{\beta}_a$ is the aerosol extinction coefficient (km^{-1}) averaged with respect to instrumental responsivity $f(v)$ over the spectral band where $f(v)$ is non-zero.

1.3 Refraction

In contrast to free space where optical rays are straight, within the atmosphere optical rays bend toward the region of higher refractive index. In addition to this bending, which occurs very generally at all elevations, certain refractive effects become

very noticeable for elevations close to the ocean surface and long paths on the order of 10 km. These effects, although more rare than molecular or aerosol effects, are possible to observe under special circumstances. They include the situation in which neighboring rays may be brought closer together than their free space counterparts (the rays are focused), or in which the opposite is true (the rays are defocused). Reflections and mirages may also occur. They cause comparatively radical redirection of the ray bundles leading to their capture when they would be lost under more ordinary conditions. Following Dion[6], we assign the symbol ρ and the name "refractance" to all these refractive effects as follows:

$$\rho(v, L, h) = \frac{P(v, L, h)}{P_{f\,s}(L)} \qquad (6)$$

Here P is the power (W) at wave number v reaching the end of a path through an ideal refractive atmosphere. The path length is L and average height is h. P_{fs} is the power that would arrive at the end of a path through free space whose length is also L. We note that, in free space, the power falls off from a point source as $1/L^2$, so that a value for ρ of unity describes the "$1/R^2$ fall off" of a point source.

Refractance is a weak function of wave number but a strong function of path length, path height, and atmospheric conditions. In contrast to molecular and aerosol transmission, which are always less than one, refractance may be greater than one.

1.4 Scintillation

So far, we have been discussing the average value of the transmission signal along an optical path. Optical scintillation, which is responsible for the twinkling of stars, also causes fluctuations of the transmission signal about its mean value. Scintillation is due to interference in the detector of two rays originating from the same point on the source. Ordinarily two such rays would propagate radially away from one another and never meet on the detector. However, random fluctuations in the refractive index of the air continually occur, and it may happen that they momentarily bend the two diverging rays toward one another and cause them to meet briefly on the detector. Since they originated from the same point on the source, they are capable of interfering, which they may do destructively or constructively depending on their relative phase.

The maximum frequency of infrared scintillation is typically 100 Hz. The variance of the fluctuating signal divided by the square of the mean signal is called the scintillation index. The signal-to-noise ratio is given by one over the square root of the scintillation index. For a 10 km path the scintillation index typically varies from 0.01 (signal-to-noise 10/1) in very still conditions (a refractive index structure constant, C_n^2, of about 1×10^{-17} m$^{-2/3}$) to 0.3 (signal-to-noise 2/1) in very turbulent conditions (C_n^2 about 1×10^{-13} m$^{-2/3}$). However, the signal-to-noise situation in strong turbulence is actually worse than the signal-to-noise ratio indicates because the scintillation has a log normal spectrum with large spikes that commonly exceed 5 times the mean.

1.5 Mean Transmission

Assuming independence of all the effects just described, the mean broad band transmission may be described by the product of the molecular transmission, the aerosol transmission, and the refractance:

$$\bar{\tau}(f, L, h) = \bar{\tau}_m(f, L) \cdot \exp\left\{-\bar{\beta}_a L\right\} \cdot \rho(f, L, h) \qquad (7)$$

Observed transmission is generally less than 100%, the free space value, but may occasionally exceed 100% when the air is clear and the refractance is large.

2. THE EXPERIMENT

During the end of March and the first two weeks of April, 1996, a field experiment in the San Diego area was held as part of the ONR sponsored program called Electro-Optical Propagation Assessment in Coastal Environments (EOPACE). This particular phase concentrated on the low altitude measurement of infrared transmission across San Diego Bay. An overhead satellite photograph of San Diego Bay is shown in figure 1. Two infrared transmission paths can be seen: a 15 km long path between the Naval Submarine Base, Point Loma and the Imperial Beach Pier and a 7 km path between the Naval Submarine Base, Point Loma and the Naval Amphibious Base, Coronado. Meteorological data were taken at all these locations and at buoys moored in the bay. The paths necessarily contained small over land segments and several tens of meters of surf at Coronado, and they passed over a jetty and sheltered water at the entrance to San Diego Harbor. These low altitude paths were often obscured by passage of Navy ships and small boats sailing in and out of the harbor. The prevailing winds in the San Diego region come from the northwest, and as a result the Point Loma receiver location is generally sheltered from the wind whereas the transmitter locations at Coronado and Imperial Beach are exposed to the wind.
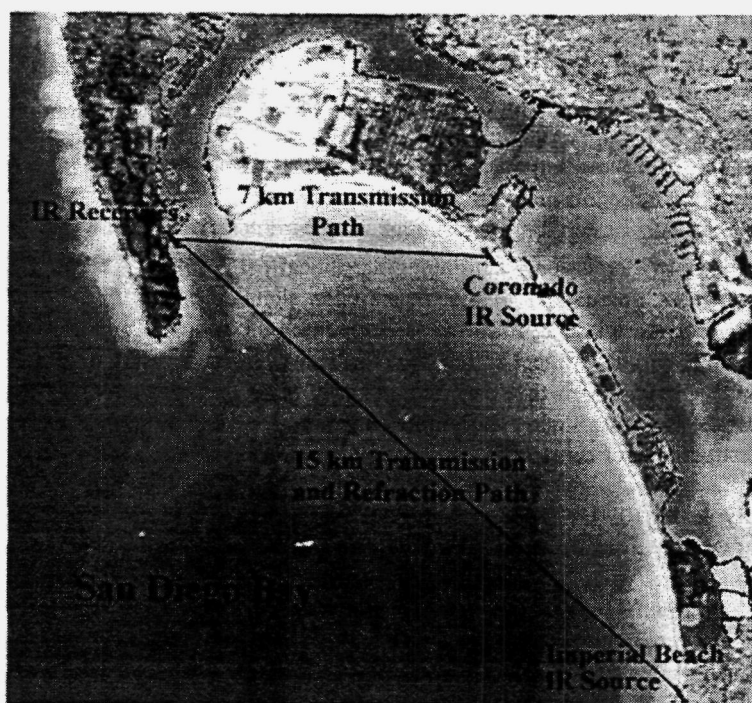

Figure 1. Satellite view of San Diego Bay showing the optical paths used during the March and April 1996 EOPACE transmission experiment.

The spectral responsivity of the equipment on each path is shown in figure 2, the experimental data are shown in figures 3 and figure 4, the molecular transmittance is shown in figure 5, and an aerosol size distribution is shown in figure 6. Times are given in decimal fractions of a Julian day local time. The data discussed here begin at day 91 (just after midnight Pacific Standard Time on 31 March 1996) and last for 13 days until day 104 (just before midnight Pacific Daylight Time on 12 April 1996). There was a change from Pacific Standard Time to Pacific Daylight Time at 2:00 A.M. on 7 April 1996, with the result that there is a one hour gap in the data between 98.08333 and 98.12500. Lindbergh field reported 0.03 inches of rain on day 92 and 0.01 inches on day 101. There was a Santa Ana episode in the middle of the experiment between 96.25 and 98.75.

Meteorological and mid wave transmission data were recorded each minute throughout the experimental period with some minor exceptions and two major exceptions: (1) when the mid wave detector was removed from the long path transmissometer to make a long wave measurement, and (2) during the failure of the computer on the long path buoy. When data were correlated with one another, a single observation was defined to consist of the various infrared and meteorological data reported at the same minute. This procedure ignored timing errors introduced by variations in the setting and running of the computer clocks, but for the examination of diurnal trends in noisy data, errors due to this procedure can be safely ignored.

3. THE EQUIPMENT

3.1 Long Path Transmissometer

An infrared transmissometer was operated over the long path by TNO. The transmitter and receiver were optically identical Newtonian reflectors consisting of a primary spherical mirror 200 mm in diameter with a focal length of 400 mm (F/2) and a rectangular secondary mirror mounted at 45° to the optical axis presenting an 85 mm x 85 mm obscuration normal to the optical axis. The active area (primary area minus secondary obscuration) of each telescope was 230 cm².

The transmitter was mounted 9 m above mean sea level on the balustrade of the lifeguard station on the Imperial Beach pier. The coordinates of the transmitter were 32° 34' 45" North latitude and 117° 08' 07" West longitude. A 900 K heat source, regulated to better than 1 K, was located in the focal plane of the transmitter primary. The source aperture was 4 mm in diameter giving the transmitter a beam divergence of 10 mrad. This rather wide beam provided the transmitter with relaxed tolerances for alignment and stability. The source was chopped at 820 Hz with a rotating blade. A reference signal for lock-in detection was transmitted by a 400 MHz radio signal from one end of the path to the other.

The receiver was mounted 5.4 m above mean sea level inside room 146 in the Bachelor Officer's Quarters at the Naval Submarine Base, Point Loma. The coordinates of the receiver were 32° 41' 03" North latitude and 117° 14' 04" West longitude from which it can be shown that the transmitter was located 14.9 km from the receiver on a bearing of 141.5° True. A long wave and a mid wave detector were alternately placed in the focal plane of the receiver primary in order to conveniently record data from each of these bands with a single telescope. Each detector remained in the receiver for hours at a time. Only the mid wave detector and data will be discussed in this paper. The mid wave HgCdTe detector, manufactured by Graseby
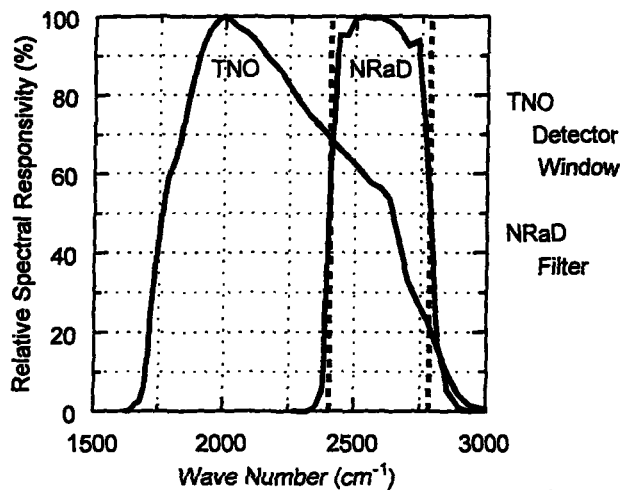
Figure 2. Relative spectral responsivity of the detector and window, labeled "TNO," used on the long path, and the warm filter, labeled "NRaD," used on the short path. For molecular predictions, the TNO responsivity was applied as shown but the NRaD responsivity was replaced by the two dashed lines shown running vertically through 50% responsivity at 2405 cm^{-1} and 2783 cm^{-1}.

Infrared[7], was 2.0 mm x 2.0 mm resulting in a 5 mrad field of view given the 400 mm focal length of the primary. The detector was placed 7 mm below a warm sapphire window and had a 60° field of view. The relative spectral responsivity of this detector-window combination is labeled "TNO" in figure 2. The peak value of detectivity, D*, at a 1 kHz chopping frequency was 4.0 x 10^{10} cm Hz$^{1/2}$ W^{-1} at a bias of 3 mA. The integration time of the lock-in was 3 s for an equivalent noise bandwidth of 1/20 Hz and a signal-to-detector noise ratio of more than 100/1. Data were sampled each second, 60 consecutive samples were averaged together, and the averaged values were reported each minute.

The long path transmissometer was calibrated[8] by a careful series of laboratory and field experiments.

3.2 Short Path Transmissometer

A second infrared transmissometer was operated over the short path by NRaD. The transmitter and receiver were Newtonian reflectors consisting of F/6 paraboloids 200 mm in diameter and elliptical secondary mirrors mounted at 45° to the optical axis. All mirror surfaces were aluminum coated. The secondary mirror obstruction was about 8% of the primary aperture in each case. The effective area (primary area minus secondary obscuration taking into account variations in primary reflectivity) of each telescope was 226 cm^2.

The transmitter was mounted 3.04 m above mean sea level on a platform near the edge of the bay at the Naval Amphibious Base, Coronado. The coordinates of the transmitter were 32° 40' 04" North latitude and 117° 09' 54" West longitude. A ¼ ohm close wound wire coil, driven by a regulated current source to an average temperature of 1130 K, was located in the primary focal plane. Ten thermocouple measurements taken at random locations across the coil face showed a variation of ± 41 K (± 1 σ), presumably because of variations in the resistivity of the wire. This translates to a radiance variation of ± 11% when the responsivity of the "NRaD" filter shown in figure 2 is taken into account. Normal to the optical axis the source filled a 9 mm x 9 mm area, giving the transmitter a beam divergence of 7 ½ mrad. The source was chopped at 960 Hz with a
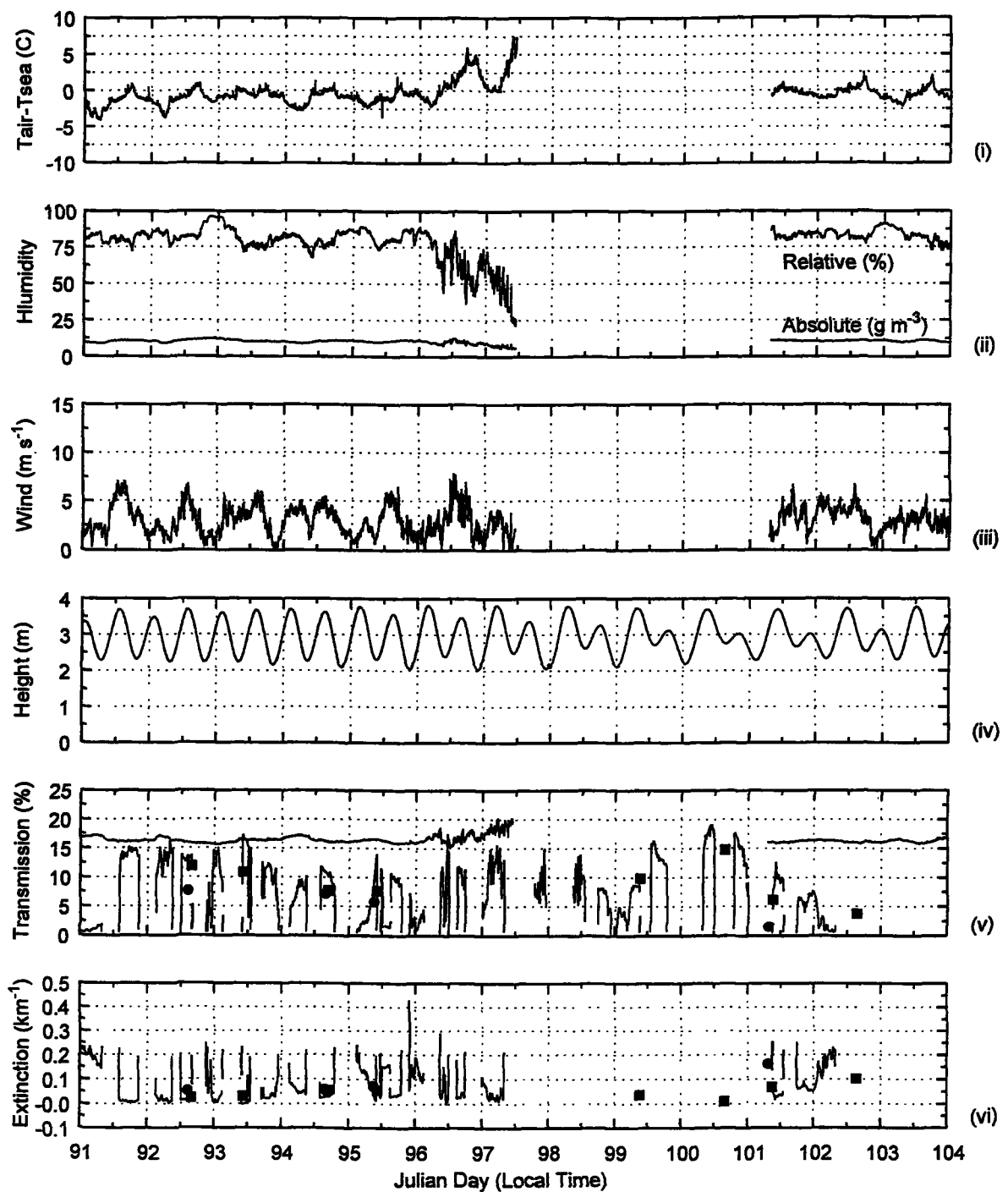
Figure 3. Meteorological and transmission data on the long path. Part (i), air-sea temperature difference. Part (ii), relative and absolute humidity. Part (iii), wind speed. Part (iv), free space mid path height. Part (v), predicted clear air transmission (flat line), measured transmission (variable line) and the product of predicted clear air and measured aerosol transmission (squares inbound, circles outbound). Part (vi), aerosol extinction inferred from transmission data (solid line) and measured along the path (squares inbound, circles outbound). The missing meteorological data were caused by a computer failure on the long path buoy.
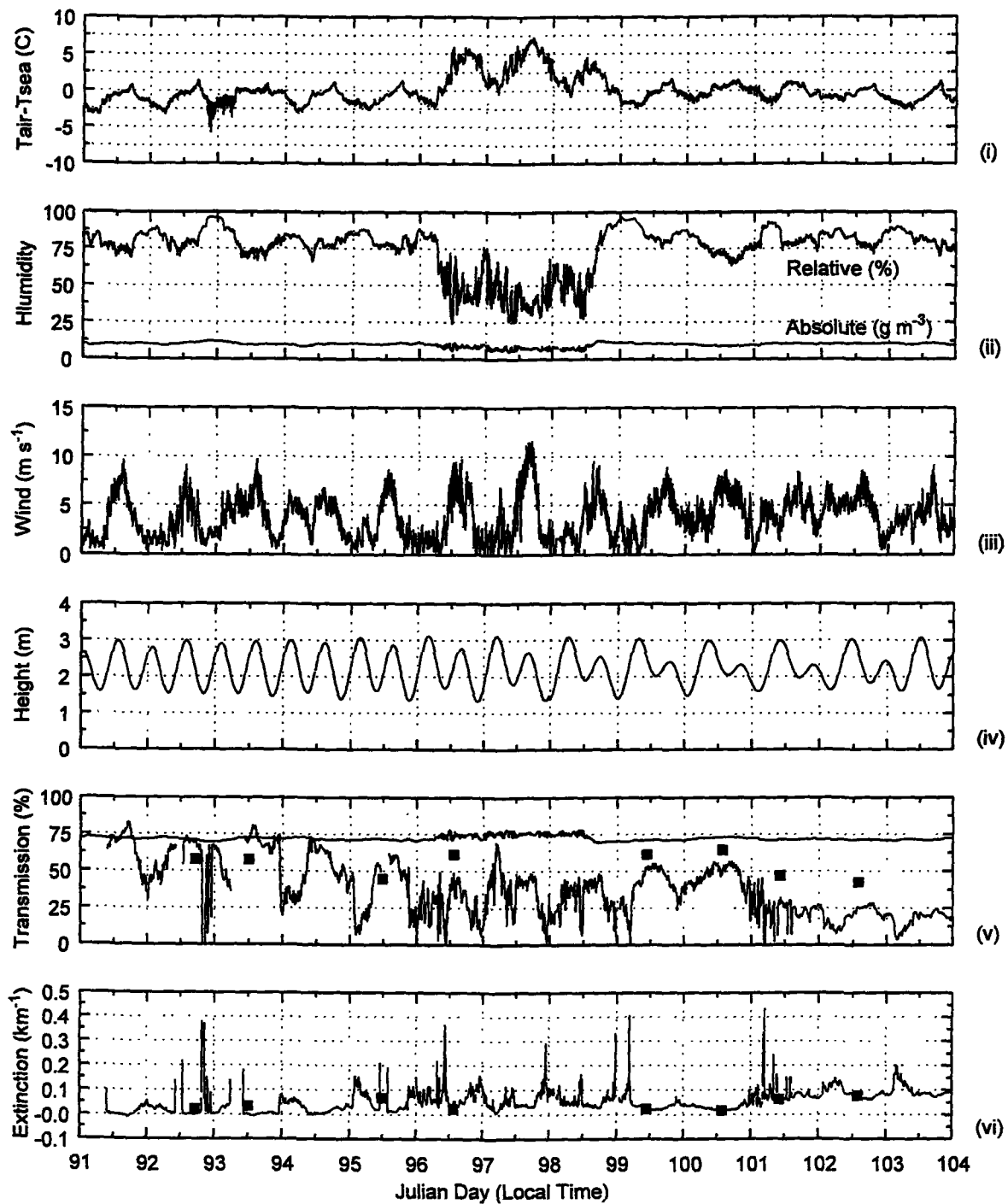
Figure 4. Meteorological and transmission data on the short path. Parts (I) to (vi) are the same as for figure 3.

rotating blade. A reference signal for lock-in detection was transmitted by a 162.1 MHz radio signal from one end of the path to the other.

The receiver was mounted 3.21 m above mean sea level inside a trailer on a concrete pad at the edge of the bay at the Naval Submarine Base, Point Loma. The coordinates of the receiver were 32° 40' 59" North latitude and 117° 14' 14" West longitude, from which it can be shown that the transmitter was located 7.0 km from the receiver on a bearing of 104° True. The mid wave detector, manufactured from InSb by Belov Technology[9], had an area of 3.0 mm x 3.0 mm resulting in a 2.5 mrad field of view given the 1200 mm focal length of the primary. The InSb detector was mounted on top of a HgCdTe long wave detector in a sandwich configuration, but the long wave detector was not used in this experiment. A warm filter with the relative spectral responsivity labeled "NRaD" in figure 2 was placed in the optical path in front of the detector. The integration time of the lock-in was 1 s with a roll-off of 12 dB/octave for an equivalent noise bandwidth of 1/8 Hz and a signal-to-detector noise ratio of more than 1000/1. Data were sampled every 6 seconds, 10 consecutive samples were averaged together, and the averaged values were reported each minute.

The short path transmissometer was calibrated absolutely to an accuracy of ±30% by the method outlined in the appendix.

3.1 Mid Path Meteorological Buoys

Two meteorological buoys were deployed in San Diego Bay during this experiment by the Boundary Layer Studies Group of the Naval Postgraduate School, Monterey. A mean meterological buoy was located at 32° 40' 24" North latitude and 117° 12' 15" West longitude near the middle of the short optical path. The mean buoy had sensors to measure mean meteorological data and sea surface temperature. A flux buoy was located at 32° 37' 40" North latitude and 117° 11' 00" West longitude near the middle of the long optical path. In addition to the same sensors as those on the mean meterological buoy, the flux buoy had a sonic anemometer to measure turbulent wind and temperature fluctuations and a motion pack and wave staff to measure buoy motion and surface wave properties. Only the mean data from each buoy system are reported here. The type of mean instrument and the height on the buoy at which each instrument was mounted are given in Table I.

Data were averaged over a 1 minute interval and reported each minute. These data are shown in figures 3 and 4 for the long and short paths respectively. As can be seen from figure 3, data from the long path buoy are missing between 97.4 and 101.3. This was caused by a computer malfunction.

Table I: Buoy Instruments and Mounting Heights.

Instrument	Measurement	Height (m) on mean met buoy	Height (m) on flux buoy
R. M. Young	Wind speed, direction	4.88	3.80
Rotronics	Air temperature, relative humidity	4.09	3.86
Everest infrared	Sea surface temperature	1.82	2.50
Barometer	Atmospheric pressure	0.38	0.22
TCM compass	Magnetic heading	0.13	0.25

3.4 Tide Predictions

The tide data shown in figures 3 and 4 were *not* measured. They were taken from a computer program[10] which predicts mean sea level for any given time and geographic location. Comparisons between this prediction and tides measured at Scripps Pier suggest that these predictions are accurate to several cm. The tide predictions for Point Loma were adjusted to give the mid path optical height above sea level as follows: A straight (free space) ray was assumed to propagate between the transmitter and receiver. Between these two points, the earth curves up by about 4 m on the long path and 1 m on the short path. This effect was be taken into account by calculating the distance between the free space ray and the surface of an ideal curved earth at mid path. The predicted tide was subtracted from this mid path height to give the heights shown in figures 3 (iv) and 4 (iv).

4. DATA PROCESSING

Transmission data were smoothed and processed to reduce the effects of ships blocking the transmission path. While operating the receivers, it was often noticed that large Navy ships and small sailboats moving in the entrance to San Diego harbor would block the optical path, momentarily reducing the transmission signal toward zero. Examination of the raw transmission data revealed isolated observations much lower than the envelope of the signal fluctuations. We assumed that these isolated lows were objects blocking the path. To reduce their influence, the data for one day were smoothed using the {357H} smoothing routine in the statistics program Stata[11], the standard deviation of the data for that day was computed, and any observations more than 3 standard deviations below the smoothed value were replaced by that smoothed value in the raw (un-smoothed) data set. The raw data with these lows removed was then smoothed anew with the {357H} algorithm, which is roughly equivalent to taking a 7 minute moving average. The processed transmission data are shown as the variable solid line in part (v) of figures 3 and 4.
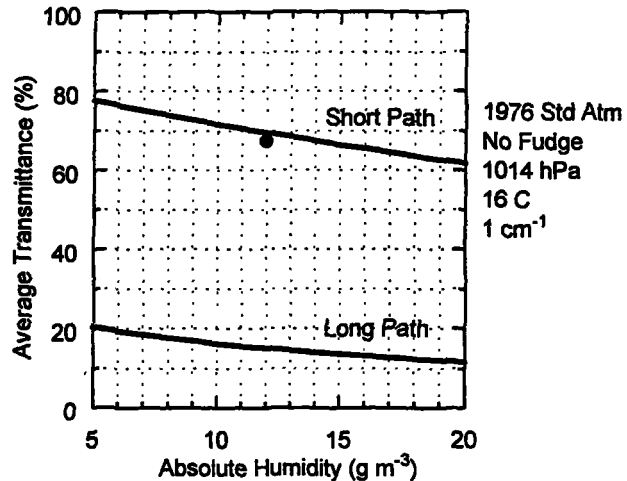
5. CLEAR AIR ANALYSIS

Figure 5. Broad band molecular transmittance as a function of absolute humidity for the responsivities and path lengths appropriate to each optical path. These results were obtained with MODTRAN 2 without the "fudge" routine. The solid circle shows the MODTRAN 3 result for the short path.

To analyze the transmission data for molecular effects, each observation of pressure (hPa), temperature (K), and relative humidity (%) at the mid path buoy were converted to absolute humidity (g m^{-3}). The absolute humidity was used in MODTRAN 2 to calculate the clear air (aerosol free) transmission corresponding to the meterological observations for that minute. This molecular prediction is shown as the flat solid line in figures 3 (v) and 4 (v).

In more detail, the transmission was predicted from the absolute humidity for a horizontal path within the 1976 U. S. Standard Atmosphere. For the long path, the TNO responsivity, shown in figure 2, was inserted into the MODTRAN 2 code and the broad band transmission was calculated from equation (3). For the short path, the NRaD responsivity shown in figure 2 was approximated by the dashed lines shown there. This amounts to replacing the actual $f(v)$ with its "top hat" version (zero below 2405 cm^{-1}, zero above 2783 cm^{-1}, and unity in between) and using equation (2). The results of this calculation for a temperature of 16 C and a pressure of 1014 hPa are shown in figure 5. The results were weakly dependent on temperature and pressure. At 12 g m^{-3} these dependencies were

$$\frac{\Delta \bar{\tau}_m}{\Delta T} \approx + \frac{0.03\%}{K}, \; long \; path$$

$$\approx + \frac{0.09\%}{K}, \; short \; path \tag{8}$$

$$\frac{\Delta \bar{\tau}_m}{\Delta P} \approx - \frac{0.02\%}{hPa}, \; both \; paths$$

During this calculation, the MODTRAN 2 subroutine "fudge" was disabled to bring the calculation into better agreement with the MODTRAN 3 calculation, shown for the short path as the solid circle in figure 5. With "fudge" enabled, results on the short path were approximately 10% lower than those shown in figure 5.

6. AEROSOL ANALYSIS

Short Path
Inbound
Time 99.444

Extinction
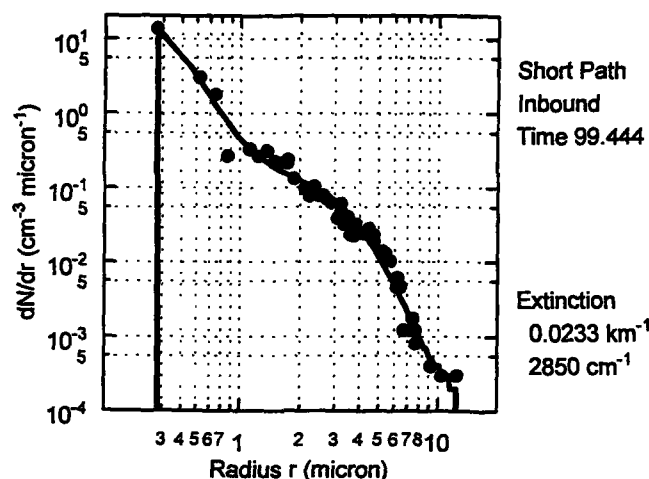0.0233 km^{-1}
2850 cm^{-1}

Figure 6. Aerosol size distribution measured between 10:25 AM and 10:55 AM Pacific Daylight time during a boat run from Coronado to Point Loma (inbound on the short path). The data were fit with a fifth order polynomial and integrated using equation (9) to give an extinction of 0.0233 km^{-1} equivalent to an aerosol transmission of 85%. The integral was truncated at the vertical lines through the smallest and largest observed radii.

Aerosols along the long and short path were measured by transporting a classical scattering aerosol spectrometer probe[12] in a small boat outbound (from receiver to transmitter) and inbound (from transmitter to receiver) along the over-water portion of each path. The boat runs occurred on 9 days out of the 13. A one-way run took about 1 hour on the long path and about ½ hour on the short path, and the aerosol size distribution was integrated for the entire outbound or inbound run. Although the mouth of the aerosol spectrometer faced toward the bow of the boat, there were occasions when the prevailing wind blew diesel exhaust from the stern past the bow, suggesting that exhaust particles might contaminate the aerosol data. Therefore, those runs for which the prevailing wind direction was within ± 30° of the path, blowing from stern to bow, were rejected. On the long path, this eliminated 5 runs, leaving 12 (an inbound run on the long path was skipped at 96.635). On the short path, all 9 outbound runs were eliminated leaving 8 inbound runs (there was a power failure at 94.582 inbound on the short path).

A representative spectrum from a single run is shown in figure 6. The spectrum shows dN/dr (cm^{-3} μm^{-1}), the number of aerosol particles per unit volume whose radii lie between r and $r + dr$ μm, as a function of particle radius. The data, shown as solid circles in figure 6, were fit with a fifth order polynomial, truncated abruptly at the minimum and maximum observed radii, and integrated according to

Mie theory using the equation

$$\overline{\beta}_a \equiv \beta_a(v) = \int_0^\infty \pi r^2 Q_a(v) \frac{dN}{dr} dr \tag{9}$$

Here $Q_a(v)$ is the dimensionless Mie efficiency factor for aerosol extinction, provided in our calculations by the Dave code[13]. As indicated in equation (9), we assumed that there was no variation of extinction over the spectral bands shown in figure 2. We always chose a wave number of 2850 cm^{-1} during the integration.

Table II gives the aerosol extinction coefficients arrived at by this method, and also shows the equivalent aerosol transmission obtained from the extinction in each case by means of equation (5). The solid symbols in figures 3 (v) and 4 (v) give the product of molecular transmission and aerosol transmission; that is, they show the values predicted by equation (7) from figure 5 and Table II assuming a refractance of one.

In addition to working forward from the aerosol size distribution to get an aerosol extinction, we may work backward from transmission measurements to get another version of aerosol extinction, provided that we assume a refractance of one. Since aerosol transmission obeys Beer's law, approximately, we may invert equation (7) to infer a band-averaged aerosol extinction coefficient. That is, we may use

$$\bar{\beta}_a = \frac{-\ln\bar{\tau} + \ln\bar{\tau}_m + \ln\rho}{L} \qquad (10)$$

to derive an aerosol extinction, independent of path length L, from the actual measured and predicted molecular transmission values. In figures 3 (vi) and 4 (vi) we show the result of this inversion when refractive effects are ignored by setting $\rho \equiv 1$.

Table II. Aerosol Extinction and Transmission at 2850 cm^{-1}.

Long Path Outbound			Long Path Inbound			Short Path Inbound		
Time Out	β_a (km^{-1})	τ_a (%)	Time In	β_a (km^{-1})	τ_a (%)	Time In	β_a (km^{-1})	τ_a (%)
92.611	0.0542	45	92.660	0.0238	70	92.724	0.0212	80
—	—	—	93.433	0.0299	64	93.507	0.0323	80
94.655	0.0578	42	94.699	0.0531	45	94.582	—	—
95.378	0.0725	34	95.429	0.0544	45	95.490	0.0675	62
—	—	—	96.635	—	—	96.560	0.0232	85
—	—	—	99.385	0.0361	58	99.444	0.0233	85
—	—	—	100.655	0.0092	87	100.574	0.0164	89
101.319	0.1631	9	101.373	0.0679	36	101.430	0.0624	65
—	—	—	102.645	0.1024	22	102.581	0.0750	59

7. CORRELATIONS

Meterological and optical properties along the two paths were correlated with one another. The results are shown in Table III, which give the Stata correlation coefficient and the number of observations involved in each correlation.

Table III. Correlations Between Long and Short Path Observations.

Observation	Coefficient	Number
Tair-Tsea	.8778	13993
Relative Humidity	.8927	13993
Absolute Humidity	.8300	14551
Wind Speed	.7474	14551
Molecular Transmission	.7863	13993
Aerosol Extinction	.7308	5178

8. DISCUSSION

From figures 3 (vi) and 4 (vi), there appears to be agreement between aerosol extinction on the two paths, and the daily variations in extinction appear to be well correlated with daily variations of the relative humidity. A useful idea associated with ocean aerosols is that that the size distribution, for example the one shown in figure 6, shifts laterally as the relative humidity increases. The shift does not progress linearly with relative humidity: it proceeds very slowly until humidities in the vicinity of 95% are reached, and then it proceeds very rapidly. Experience with the integration involved in equation (9) has taught that, roughly speaking, the most influential particles are those with radii near the wavelength corresponding to the wave number ν which remains fixed during the integration. As a result of the lateral shift produced by changes in the relative humidity, the number of particles with radii near the wavelength changes, causing a change in the extinction. Careful examination of figures 3 and 4, parts (ii) and (vi), shows that large spikes in extinction correspond well with excursions of

relative humidity close to 100%. The most plausible explanation for this is a growth of aerosols culminating, perhaps, in patches of fog along the path.

An noteworthy feature of figures 3 (iv) and 4 (iv) is the almost constant value of predicted molecular transmittance. On the long path the molecular transmittance was 16.5 ± 0.6% (14555 observations); on the short path it was 72.0 ± 1.6% (19220 observations). This was in spite of the Santa Ana episode, in the middle of this 13 day period, when the mid day air-sea temperature difference doubled and changed sign to about + 5° C and the relative humidity fell by a factor of 2 to about 50%. Close examination of these figures shows that the shape of each molecular transmittance curve is the mirror image of the shape of each absolute humidity curve, a result which should be expected given the fact, stated in Section 5, that molecular transmittance is almost completely determined by absolute humidity. The reason that molecular transmittance does not vary greatly is explained by the rather mild dependence, shown in figure 5, of molecular transmittance on absolute humidity. So it appears that a useful practical approximation for San Diego Bay in April 1996 is that the mid wave molecular transmission was 17% on the 14.9 km path and 72% on the 7.0 km path. (We remind the reader that these results may not be converted with Beer's Law to an extinction for application to other ranges.)

The predicted molecular transmission shown in figures 3 (iv) and 4 (iv) generally provides an upper limit to the measured transmission, which is reassuring. However, on the short path there *are* hours during the afternoon of days 95 and 97 when the measured transmission is as much as 10% above the predicted clear air value. This reflects either (1) experimental error in the transmissometer calibration (see the appendix) or (2) actual clear air accompanied by a refractance greater than one (see the next paper in these proceedings). The same comment also applies to the difference between the measured transmission (variable solid line) and the product of molecular and aerosol transmission (solid symbols) in figures 3 (v) and 4 (v); that is, these differences, which are within experimental error, may be due to refraction.

9. CONCLUSION

We have reported 13 consecutive days of mid wave infrared transmission data. Observations were made once a minute along horizontal paths above San Diego Bay at elevations of several meters, depending on the tide. There were two paths: a long 14.9 km path on a bearing of 141.5° True from Point Loma, California, and a short 7.0 km path on a bearing of 104° True from the same location. Mid path buoys supplied meterological data coincident with each transmission observation. Measurements of aerosol size distribution were made with an aerosol spectrometer transported by boat along each path.

Meterological and transmission data on the two paths were correlated to more than 0.7 in the course of more than 5000 observations.

The transmission data were analyzed with MODTRAN and Mie theory neglecting refraction. Molecular (clear air) transmission, as predicted by MODTRAN 2 from the buoy data, was remarkably constant at 17 ± 0.6% on the long path and 72 ± 1.6% on the short path. On the other hand, aerosol transmission, obtained by dividing measurements by the predicted molecular transmission, varied widely between 0% and 100%. Aerosol transmission had a strong daily component which appeared well correlated with relative humidity, suggesting that daily variations in mid wave infrared transmission are dominated by aerosols in San Diego Bay. This supposition is further strengthened by the fact that the extinction obtained from directly measured aerosol size distributions agrees well with the extinction inferred from transmission.

ACKNOWLEDGEMENT

REFERENCES

1. L. Forand, D. Dion, C. R. Zeisse, S. G. Gathman, and A. N. de Jong, "Refraction Effects on Low-Elevation Transmission Measurements at EOPACE," paper 3125-12 of these proceedings.
2. A. N. de Jong and G. de Leeuw, "Low-Elevation Transmission Measurements at EOPACE part III: Scintillation Effects," paper 3125-13 of these proceedings.

3. C. R. Zeisse, "Relative Spectral Responsivity of Two AGEMA Infrared Scanning Cameras," *NRaD Technical Report 1699*, pp. 1-34, 1995.

4. A. Berk, L. S. Bernstein, and D. C. Robertson, "MODTRAN: A Moderate Resolution Model for LOWTRAN 7," *Air Force Geophysics Laboratory Report GL-TR-89-0122*, pp. 1-42, 1989.

5. E. P. Shettle, private communication.

6. D. Dion, "Refraction Effects on EO System Detection Ranges in Coastal Environments," *Proceedings AGARD-CP-567 of the AGARD Conference on Propagation Assessment in Coastal Environments*, pp. 15-1 to 15-9, 1995.

7. Graseby Infrared, 12151 Research Parkway, Orlando, FL, 32826-3207.

8. A. N. de Jong and P. J. Fritz, "EOPACE Transmission Experiments Spring 1996; Preliminary Results," *TNO Report FEL-96-A090*, pp. 1-17, A.1-A.29, 1996.

9. Belov Technology Co. Inc., 345 Sandford Street, New Brunswick, NJ 08901.

10. Tides and Currents for Windows, version 2.0b, Nautical Software, 14657 SW Teal Boulevard, Suite 132, Beaverton, OR 97007.

11. Intercooled Stata for Windows 95, version 5, Stata Press, 702 University Drive East, College Station, TX 77840. The {357H} smoothing routine applies a span 3 smoother, followed by a span 5 smoother, followed by a span 7 smoother, followed by a Hanning smoother. A span 3 smoother replaces an observation at t by the median of observations at t-1, t, and t + 1.

12. Model CSASP-100-HV, Particle Measuring Systems Incorporated, 5475 Airport Boulevard, Boulder, CO 80301-2339.

13. J. V. Dave, "Subroutines for Computing the Parameters of the Electromagnetic Radiation Scattered by a Sphere," *IBM Palo Alto Report 320-3237*, pp. 1-65, 1968.

APPENDIX: ABSOLUTE CALIBRATION OF THE NRaD TRANSMISSOMETER

The voltage corresponding to free space transmission at full range was 6.32 ± 1.9 mV for the NRaD transmissometer. This was determined by placing the transmitter in front of the receiver in the laboratory and using the law of conservation of radiance to predict the free space voltage at full range.

We make the following four assumptions:

1. The voltage out of the detector is proportional to the optical power falling on the detector.

2. The image of the source underfills the detector both in the lab and in the field.

3. The atmosphere in the laboratory is completely transparent within the spectral pass band of the instrument.

4. After removal of two calibration apertures (a pinhole and a mask), nothing changes between the lab calibration and the field measurement except the range.

In the laboratory, the transmitter and receiver face one another with a nominal separation of 10 to 20 cm between the end of the transmitting telescope and the beginning of the receiving telescope. A pinhole with an area of $A_{pinhole}$ was placed in the focal plane of the transmitter directly in front of the black body source. A mask with an area A_{mask} was placed in the space between the two telescopes. Let the radiance of the black body be N, the combined in band reflectivity of all four reflecting surfaces (two primary mirrors and two secondary mirrors) be R, and the focal length of the transmitting primary be f. Then the laboratory voltage V_L is proportional to the laboratory power P_L which is found from the radiance at the pinhole to be

$$V_L \propto P_L = N A_{pinhole} \frac{A_{mask}}{f^2} R \qquad \text{(A-1)}$$

The value of V_L is recorded in the laboratory by the same electronics used in the field. Then the pinhole and mask are removed and the equipment is moved into the field.

In the field, the transmitter and receiver still face one another but now they are separated by the full range for the field measurement, L. Let the clear area of the transmitter (receiver) primary be denoted by A_{Tx} (A_{Rx}) and let the in band atmospheric transmission be denoted by τ. Then the field voltage V_F is proportional to the field power P_F which is found from the radiance at the transmitting primary mirror to be

$$V_F \propto P_F = N\,A_{Tx}\,\frac{A_{Rx}}{L^2}\,R\tau \tag{A-2}$$

Taking the ratio of these two equations we find the following correspondence between field voltage and atmospheric transmission:

$$V_F = \alpha\,V_L\,\tau,$$

$$\alpha \equiv \left(\frac{f}{L}\right)^2 \frac{A_{Tx}\,A_{Rx}}{A_{pinhole}\,A_{mask}} \tag{A-3}$$

The values of these parameters for the April 1996 calibration are given in Table 1. The voltages given in the first paragraph of this appendix are equal to αV_L. In other words, they are the value V_F would have in free space where there are no molecules, no aerosols, and all the rays are straight.

Table A-1

f	1235	mm
L	7.0	km
$D_{pinhole}$	0.300	mm
D_{mask}	10.2 ± 0.1	mm
A_{Tx}	226	cm^2
A_{Rx}	226	cm^2
α	2.75	—
V_L	2.3	mV

We analyzed the random and systematic errors for the above calibration method, including, for example, the variation of temperature across the source coil, and arrived at an accuracy for this procedure of $\pm 30\%$. This percentage has been applied to the average signals for free space transmission given in the first paragraph of this appendix to give the "$\pm$" signal values. An accuracy of 30% means that a measured transmission of 10% could, in truth, be anywhere from 7% to 13%. Or, a measured transmission of 70% could actually be anywhere from 50% to 90%.

Propagation and Imaging through the Atmosphere

Luc R. Bissonnette
Christopher Dainty
Chairs/Editors

29–31 July 1997
San Diego, California

P

Volume 3125